ADVANCED FUNCTIONAL MATERIALS
www.afm-journal.de

Distinguishing the Importance of Fullerene Phase Separation from Polymer Ordering in the Performance of Low Band Gap Polymer:Bis-Fullerene Heterojunctions

*Huipeng Chen, Yu-Che Hsiao, Jihua Chen, Bin Hu, and Mark Dadmun**

One way to improve power conversion efficiency (PCE) of polymer based bulk-heterojunction (BHJ) photovoltaic cells is to increase the open circuit voltage (V_{oc}). Replacing PCBM with bis-adduct fullerenes significantly improves V_{oc} and the PCE in devices based on the conjugated polymer poly(3-hexyl thiophene) (P3HT). However, for the most promising low band-gap polymer (LBP) system, replacing PCBM with ICBA results in poor short-circuit current (J_{sc}) and PCE although V_{oc} is significantly improved. The optimization of the morphology of as-cast LBP/bis-fullerene BHJ photovoltaics is attempted by adding a co-solvent to the polymer/fullerene solution prior to film deposition. Varying the solubility of polymer and fullerene in the co-solvent, bulk heterojunctions are fabricated with no change of polymer ordering, but with changes in fullerene phase separation. The morphologies of the as-cast samples are characterized by small angle neutron scattering and neutron reflectometry. A homogenous dispersion of ICBA in LBP is found in the samples where the co-solvent is selective to the polymer, giving poor device performance. Aggregates of ICBA are formed in samples where the co-solvent is selective to ICBA. The resultant morphology improves PCE by up to 246%. A quantitative analysis of the neutron data shows that the interfacial area between ICBA aggregates and its surrounding matrix is improved, facilitating charge transport and improving the PCE.

1. Introduction

Organic photovoltaic (OPV) devices based on the bulk heterojunction (BHJ) concept of blends of conjugated polymers and fullerenes have attracted significant interest for sustainable solar energy conversion due to their low-cost, light-weight, flexible and ease of processing.[1–5] The power conversion efficiency (PCE) of these devices has increased rapidly in recent years, which has been primarily due to the development of novel donor polymers, while less attention has been paid to the importance of the fullerene structure on device performance. Other than [6,6]-phenyl-C_{61}-butyric acid methyl ester (PCBM), the most widely reported fullerene in OPV devices is a bis-fullerene, Indene-C_{60} bisadduct (ICBA).[6,7] For the well-studied poly(3-hexylthiophene) (P3HT) system, replacing PCBM with bis-adduct fullerenes (i.e., ICBA) raises the lowest unoccupied molecular orbital (LUMO) lever of the acceptor, which in turn improves the open circuit voltage (V_{oc}) and power conversion efficiency (PCE) in P3HT-based devices.[6,7] However, when blended with more promising low band gap polymers, ICBA provides very poor short circuit current (J_{sc}) and PCE, although the desired large V_{oc} is always attained.[8–13] For instance, OPV devices with an active layer that consists of poly(di(2-ethylhexyloxy)benzo[1,2-b:4,5-b′]dithiophene-co-octylthieno[3,4-c]pyrrole-4,6-dione) (PBDTTPD)/PCBM bulk heterojunctions exhibit a PCE of 7.3%; while replacing PCBM with ICBA in these devices results in a PCE of 2.7%.[10] This poor performance is associated with either poor morphology or hindered charge transport in the active layer.[8–13] However, these reported values are only based on the as-cast low band-gap polymer (LBP):ICBA device, where there is very little control of the morphology.[8–13] As J_{sc} and PCE strongly depend on the morphology, the high V_{oc} might translate into dramatic improvements in power conversion efficiencies if the morphology of the LBP:ICBA mixture can be rationally controlled. Unfortunately, little work has been done to optimize the morphology of these systems after film deposition.

Dr. H. P. Chen, Prof. M. Dadmun
Department of Chemistry
University of Tennessee
Knoxville, TN 37996, USA
E-mail: Dad@utk.edu
Dr. Y.-C. Hsiao, Prof. B. Hu
Department of Materials Science and Engineering
University of Tennessee
Knoxville, TN 37996, USA
Dr. J. H. Chen
Center for Nanophase Materials Sciences
Oak Ridge National Lab
Oak Ridge, TN 37831, USA
Prof. M. Dadmun
Chemical Sciences Division
Oak Ridge National Lab
Oak Ridge, TN 37831, USA

DOI: 10.1002/adfm.201401419

© 2014 WILEY-VCH Verlag GmbH & Co. KGaA, Weinheim

The failure of thermal annealing to improve device performance in LBP:fullerene systems has been widely reported.[14–16] An alternative approach that is used to improve device performance is to add a second solvent into the LBP:fullerene mixture solution before deposition, where the solvent additive usually evaporates slowly and selectively solubilizes the fullerene.[14,17,19] One of the most well-studied LBP:fullerene systems is Poly[2,6-(4,4-bis-(2-ethylhexyl)-4*H*-cyclopenta[2,1-*b*;3,4-*b*′]dithiophene)-*alt*-4,7(2,1,3-benzothiadiazole)] (PCPDTBT):PCBM, whose efficiency increases from 1.7% up to 4.6% with the addition of a second solvent prior to film deposition.[14] PCBM aggregation and an increase of PCPDTBT ordering in the final film have been shown to occur with the presence of the second solvent.[14] These structural changes result in an improvement in charge transport, which translates to improved device performance.[14] However, these reports only focus on the behavior of the LBG:PCBM and the impact of a second solvent on a bulk heterojunction with bis-fullerene electron acceptors has not been reported. Furthermore, these previous studies only examine solvent additives in which the fullerenes are selectively soluble, while the addition of solvents in which the polymer is selectively soluble are lacking.

Therefore, in this work, we examine the effect of the addition of a second solvent and the solubility of the polymer and fullerene in the second solvent on the morphology and function of PCPDTBT:ICBA bulk heterojunctions. Two solvents with varying PCPDTBT and ICBA solubility are selected as the second solvent: one in which ICBA is selectively soluble, 2-chlorophenol (CP); the other in which PCPDTBT is selectively soluble, bromobenzene (BB). The evolution of the in-plane and vertical morphology of the bulk heterojunction is examined by small angle neutron scattering and neutron reflectometry, respectively. Neutron scattering is a powerful technique to monitor the detailed morphology of polymer:fullerene systems, as it provides sufficient contrast between polymer and fullerene.[20–22] The effect of the second solvent on the polymer ordering is examined by UV–Vis. The results provide the intricate relationship between solvent quality, morphology, and performance for LBP:bis-fullerene mixtures with the addition of a second solvent in the solution prior to deposition. This work shows that the performance of the device can improve significantly with the addition of the second solvent, and correlates this performance improvement to distinct morphological changes. These changes include increased phase separation of the fullerene with no alteration to the polymer ordering. These results, therefore, unequivocally demonstrate that the phase separation of the fullerene is crucial to device optimization. This novel method is also broadly applicable to other LBP:bis-fullerene OPV devices, and provides a facile approach to improve the performance of LBP:bis-fullerene based OPV devices.

2. Results

The orientational order of the polymer in bulk heterojunctions is one of the key factors that impacts device performance.[14,23–25] Thus, UV–Vis spectroscopy was used to monitor how the solvent quality of the co-solvent alters the local order of the PCPDTBT in these samples. A red shift in the UV–Vis absorption peak is associated with either an interchain-delocalization or a planarization of the polymer backbone, resulting in an increased π–π conjugation length and a higher degree of ordering, which facilitates hole transport.[14,23–25] The UV–Vis spectra of all the samples are shown in **Figure 1**, where the abbreviations and descriptions of samples that were studied are shown in **Table 1**. As can be seen in this figure, all samples show the same absorption spectra, indicating that there is no change of polymer ordering in the deposited films with the variation of the solvent quality during deposition.

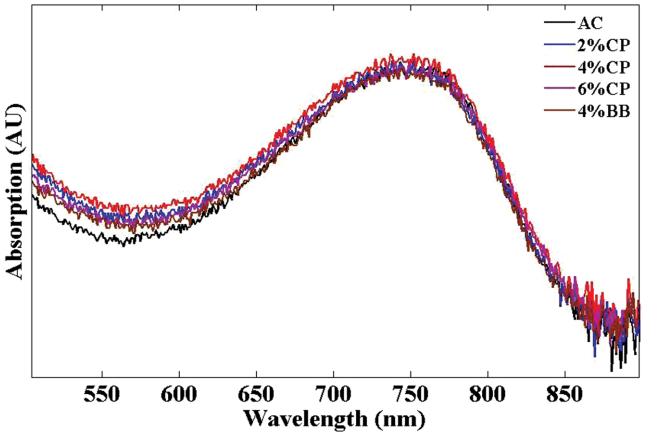

Figure 1. UV–Vis spectra for all the samples.

The vertical morphology is another key factor that impacts the device performance. An acceptor rich layer located at the air surface (near the cathode) and a donor rich layer located at the substrate (near the anode) is often presented as a morphology that will improve charge collection for a regular device.[26,27] To determine the change in depth profile with solvent quality, neutron reflectometry was employed to probe the vertical morphology of all samples. **Figure 2** shows the experimentally determined specular neutron reflectivity, as well as that of the fitted model for all the samples. The high quality of the model fits can be seen more clearly in the reflectometry curves plotted as Rq^4 as a function of q. The reflectometry curves are found to slightly change with the addition with a second solvent, which indicates a modification of the depth profiles of the components with addition of the second solvent. The thickness of the sample cast from a solution with 4% CP and the sample cast from solution with 4% BB are slightly thinner than the sample

Table 1. Abbreviation and description of samples.

Abbreviation	Description
AC	Sample from 100% ODCB
4%BB	Sample from ODCB with 4% bromobenzene
2%CP	Sample from ODCB with 2% 2-chlorophenol
4%CP	Sample from ODCB with 4% 2-chlorophenol
6%CP	Sample from ODCB with 6% 2-chlorophenol

© 2014 WILEY-VCH Verlag GmbH & Co. KGaA, Weinheim

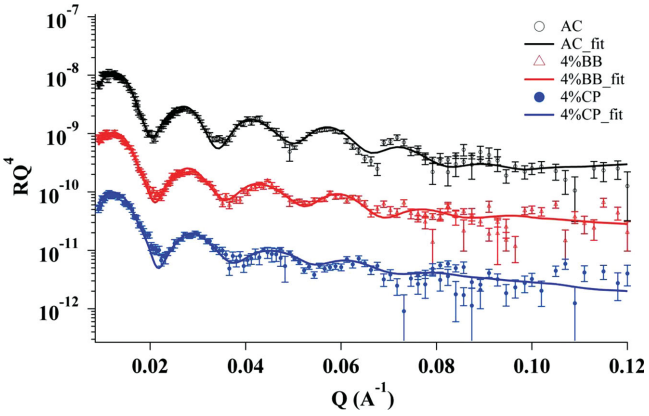

Figure 2. Reflectivity curves of the samples that are cast from 100% ODCB, 4%BB or 4% CP. The lines are fits to model scattering density profiles.

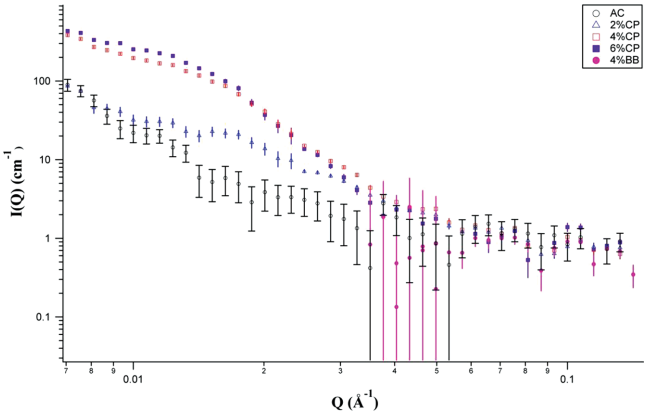

Figure 4. The absolute small angle neutron scattering intensity of all the samples.

that is cast from 100% ODCB (AC), so the resultant depth profiles are normalized to its thickness and are shown in **Figure 3**. The thicknesses of the samples are 400 Å, 390 Å, and 380 Å for the AC, 4% BB, and 4% CP samples, respectively. In this figure, $z = 0$ corresponds to the air-film interface while $z = 1$ corresponds to the film-silicon interface. Inspection of this depth profile shows that a plateau region with constant ICBA concentration exists at $z \approx 0.4$-0.7 in the sample that is cast from 100% ODCB (AC). This portion of the film is not impacted by the air interface or silicon surface. Selective segregation of ICBA to the silicon surfaces is observed in this AC thin film. Enhanced segregation of ICBA to the silicon surface and a depletion of ICBA at the air surface are observed when 4% BB, in which PCPDTBT is selective soluble, is added to ODCB. An opposite modification is observed when 4% CP, in which ICBA is selective soluble, is added to ODCB. In this sample (4% CP), a depletion of ICBA at the silicon surface and enhanced segregation of ICBA to the air surface are observed.

Reflectometry, however, only provides information on the vertical morphology of these samples, but does not provide information on the in-plane morphology that is formed when a second solvent is added to the depositing solution. Thus, small angle neutron scattering (SANS) was employed to provide information on the alteration of the in-plane morphologies of the samples with the addition of the second solvent to the depositing solution. The SANS curves of all of the samples are presented in **Figure 4**. The scattering intensity in these curves is proportional to the square of the difference of the scattering length density of the scattering object and its surroundings. Thus, the scattering is very weak if there is no or very little phase separation. The scattering of the sample that is cast from 100% ODCB (AC) sample is very weak, which is consistent with previous reports that the as-cast PCPDTBT/PCBM films from 100% ODCB consist of a fairly homogeneous distribution of the fullerene and polymer in this film.[14] An even weaker scattering is observed when the solvent contains 4% BB, which indicates a better dispersion of the ICBA and PCPDTBT in this sample (4% BB), where almost all the ICBA appears to be fairly homogeneously dispersed in PCPDTBT. A significant change of scattering intensity is observed when the depositing solution contains CP, which is selectively soluble to ICBA, as the scattering intensity increases with an increase of CP concentration. This increase in scattering intensity qualitatively indicates that one component is phase separating during deposition, where the Supporting Information describes the analysis which verifies that the phase separated domains are ICBA.

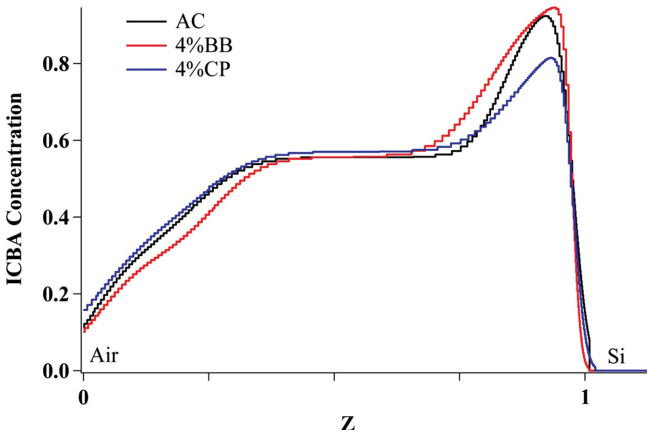

Figure 3. ICBA depth profile of AC, 4% CP and 4% BB samples as determined from the reflectivity curves shown in Figure 2 and then normalized with the actual thickness of each sample.

To more quantitatively analyze the scattering patterns to obtain structural information from the SANS curves, a detailed analysis of SANS curves is needed. In neutron scatting, the scatting intensity is proportional to $(b_1 - b_2)^2$ and the form factor ($P(Q)$) of the scattering object, $I(Q) \sim (b_1 - b_2)^2 P(Q)$. $P(Q)$ defines the shape of the scattering curve and is associated with the shape and size of domains. The scattering curves of the samples in which CP is used were fit with the assumption that the form factor is modeled by the Schulz sphere model, shown in **Figure 5**, which describes a two-phase system that consists of spherical domains with a Schulz size distribution dispersed in a surrounding matrix.[28] The Schulz sphere model has been successfully used to describe the dispersion of PCBM aggregates in the P3HT rich phase of P3HT/PCBM samples and also in the PCPDTBT rich phase of PCPDTBT/PCBM samples.[22,29,34]

Using a similar analysis to that of our previous work,[34] the detailed structure of the samples is obtained. This detailed

© 2014 WILEY-VCH Verlag GmbH & Co. KGaA, Weinheim

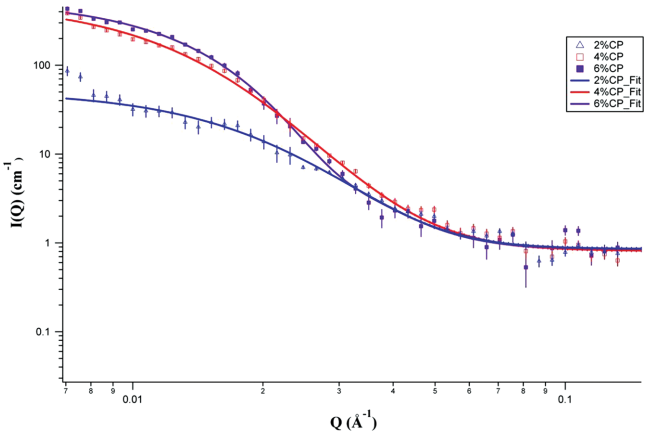

Figure 5. Fit of the structure factor of the samples in which CP is used as a second solvent to the scattering of a Schulz sphere. Parameters extracted from these fits are given in Table 2 and Table S2 (Supporting Information).

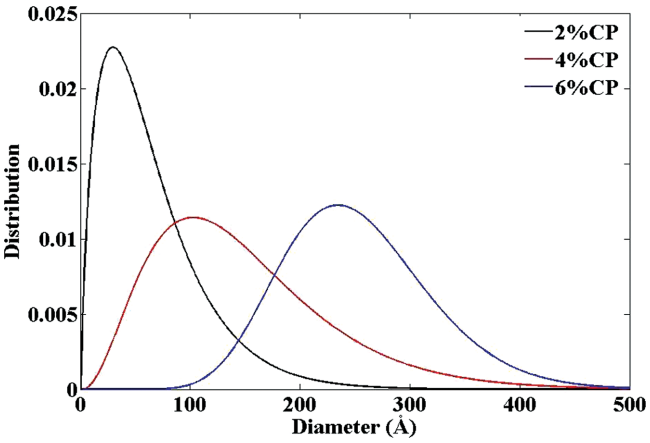

Figure 6. Size distribution of ICBA aggregates in the samples when CP is used as a second solvent.

analysis is described in the Supporting Information, and provides the volume fraction of ICBA aggregates, average diameter of the ICBA aggregates, and the size distribution and polydispersity of the ICBA aggregates. The results are shown in **Table 2**, while the size distribution of the ICBA aggregates is shown in **Figure 6**. The active layer consists of a film that contains 7.7 volume percent ICBA aggregates that are 64 Å in diameter with a polydispersity of 0.74 when 2% CP is added as a co-solvent. The volume fraction and diameter of the ICBA aggregates increases, while the polydispersity decreases, with an increase in the amount of CP co-solvent added. For instance, the active layer consists of 15.9 volume percent ICBA aggregates that are 253 Å in diameter with a polydispersity of 0.27 when 6% CP is added as co-solvent. Moreover, from these structural characteristics, the specific interfacial area (S/V) between the ICBA aggregates and its surrounding matrix can be calculated by Equation S4 (Supporting Information), where these values are shown in Table 2. These results clearly show that this parameter first increases and then decreases with an increase of CP concentration. The maximum specific interfacial area is attained when 4% CP is added as a co-solvent.

Hence, the results reported above clearly document that the morphology of as-cast PCPDTBT:ICBA films is strongly impacted by the presence of a co-solvent in the depositing solution and the solubility of the fullerene and polymer in that co-solvent. The ICBA and PCPDTBT are dispersed more effectively in a film that is cast from a solution that contains 4% BB, which is accompanied by a depletion of ICBA at the air surface and a segregation of ICBA to the silicon surface. BB is selectively soluble to the polymer. On the contrary, ICBA aggregates are formed, ICBA segregates to the air surface and is depleted at the silicon surface when CP, a preferred solvent for the ICBA, is added as a co-solvent. Moreover, the volume fraction and size of the ICBA aggregates increases and the polydispersity of the ICBA aggregates decreases with an increase of CP in the depositing solution.

In order for this information to be most useful, these structural changes must be correlated to OPV performance. With this in mind, the photovoltaic properties of all the samples were determined, as shown in **Table 3**. The power conversion efficiency (PCE) of the sample that is cast from 100% ODCB is only 1.21% and a significant decrease of PCE is found when bromobenzene is added as a co-solvent to the solution before deposition. However, the addition of CP as a co-solvent to the solution before deposition increases the short-circuit current (J_{sc}). The best device found in these studies is formed when the active layer is deposited from a solution that contains 4% CP, where the PCE increases to 4.23%, which is comparable to the best PCE of a PCPDTBT:PCBM device.[14] The electron mobility from space charge limited current (SCLC) measurements is presented in the supplemental information, shown in Table S3 (Supporting Information). These results demonstrate that the electron mobility exhibits consistent trends with J_{sc} and PCE, where the 4% CP sample has the highest electron mobility.

Table 2. Structure parameters obtained from Schulz sphere model: volume fraction of ICBA aggregates (φ); Mean diameters of ICBA aggregates; Polydispersity of the size of ICBA aggregates; Specific interfacial area between ICBA aggregates and its surrounding maxtrix (S/V).

Sample	Φ [%]	mean diameter [Å]	polydispersity (sig/avg)	S/V [cm^{-1}]
2%CP	7.7	64	0.74	344 627
4%CP	15.6	146	0.55	398 608
6%CP	15.9	253	0.27	331 130

Table 3. Device performance at standard AM-1.5 illumination.

	V_{oc} [V]	J_{sc} [mA/cm]	FF [%]	PCE [%]
AC	0.84	2.52	60	1.21
4% BB	0.84	2.26	36	0.69
2% CP	0.84	6.55	60	3.29
4% CP	0.84	7.55	65	4.23
6% CP	0.84	5.75	59	2.89

© 2014 WILEY-VCH Verlag GmbH & Co. KGaA, Weinheim

3. Discussion

Low band gap polymer (LBP):fullerene mixtures are some of the most promising organic photovoltaic active layers, yet further improvement in device performance of these materials is difficult because there is little systematic control of its morphology. For instance, replacing PCBM with ICBA in LBP systems increases the V_{oc}, which if all else were equal, should improve device performance. Unfortunately, most LBP:bis-fullerene active layers exhibit inferior performance to LBP:PCBM active layers. As the morphology of the active layer in an OPV device dramatically impacts its photovoltaic performance, a careful modification of morphology may provide the key to translating the high V_{oc} of the bis-fullerene to improved power conversion efficiency. The results presented here clearly demonstrate that inclusion of a co-solvent prior to film deposition alters the morphology of the resultant LBP:ICBA film, which in turn improves the power conversion efficiency of this LBP:ICBA bulk heterojunction.

Moreover, the results show that a judicious choice of solvent quality of the co-solvent can also dramatically alter the morphology of the active layer. A more homogeneous dispersion of PCPDTBT and ICBA in the film can be achieved when bromobenzene, which is selective to the polymer, is added as a co-solvent. The addition of 2-chlorophenol as a co-solvent, which is selective to ICBA, forms a film with ICBA phase separation. The volume fraction and size of the ICBA aggregates increases, while the size polydispersity of the ICBA aggregates decreases, with an increase in the amount of CP as the co-solvent in the solution prior to deposition. Surprisingly, adding a second solvent in which ICBA is selective soluble causes ICBA aggregates, which indicates that the interactions between PCPDTBT and ICBA dominate the deposition processing. This result is consistent with previous PCPDTBT:PCBM work, where PCBM aggregates are found when the PCPDTBT:PCBM active layer is annealed in a solvent vapor in which PCBM is selectively soluble.[34]

These morphology changes, in turn, impact its ability to act as an active layer in an organic photovoltaic device. The sample in which 4% BB is added as a co-solvent significantly decreases the PCE of the resultant active layer, which is certainly associated with the better dispersion of ICBA in PCPDTBT and the change of its depth profile. A bis-fullerene acceptor rich layer located at the air surface (near the cathode) and a polymer donor rich layer located at the substrate (near the anode) is often suggested to improve charge collection for a regular device. However, adding 4% BB creates a depletion of bis-fullerene near the air surface and enhanced segregation of ICBA near silicon surface, which inhibits electron extraction, resulting in a decrease of PCE. The morphologies that are formed when CP is used, however, do improve device performance. A morphology with a large amount of ICBA aggregates is formed when CP is used as the co-solvent. Clearly, the phase separation of ICBA facilitates electron transport, resulting in an increase of PCE.

More importantly, this work is a unique example in which fullerene aggregates form without a change in the polymer ordering. Previous reports show that an 'improved morphology' is always accompanied with an improvement of polymer ordering, making it difficult to determine the relative importance of fullerene phase separation and polymer ordering in the device performance.[14,23,30–33] The fullerene phase separation may be present or absent in these 'improved morphologies'.[14,30–33] Although some papers predict that fullerene phase separation will facilitate charge transport, the importance of fullerene phase separation in optimizing the performance of LBP:fullerene bulk heterojunctions is still not clear. This work however is a unique example that clearly documents the importance of fullerene phase separation in charge transport and device performance. This is because in these systems, the fullerene phase separation occurs in the absence of a change in polymer ordering, providing the morphological control required to separate these two morphological features in charge transport. Moreover, the results also show that the specific interfacial area between fullerene aggregates and its surrounding matrix is a vital parameter in optimizing PCE, where the S/V correlates very well to the observed device PCE.

One benefit of the presence of the mixed phase is that it provides abundant donor/acceptor interfacial area, which readily allows the dissociation of excitons to individual electrons and holes. However, this mixed phase also means that the transport of these charge carriers to the electrodes is not as efficient as in pure phases. This is because the electrons and holes co-exist in the mixed phase, increasing the possibility of bimolecular recombination. The presence of fullerene aggregates therefore appears to facilitate electron transport, thereby reducing bimolecular recombination. Moreover, the increase of specific interfacial area between the fullerene aggregates and its surrounding matrix provides more pathways connecting the mixed phase and ICBA aggregates, enabling the escape of electrons from the "slow" and "dangerous" mixed phase to the "fast" and "safe" ICBA pure phase, resulting in an increase of short-circuit current and PCE. Furthermore, the results above show a significant increase of J_{sc} and PCE that correlates to a modest increase of electron mobility, which indicates that the morphology change in the 4%CP sample results in a significant enhancement of the yield for long-lived free carrier generation and a decrease of bimolecular recombination.

4. Conclusion

The results presented in this manuscript demonstrate that the morphology of LBP:ICBA mixtures can be efficiently controlled during film deposition by the judicious addition of a co-solvent. SANS experiments demonstrate that a better dispersion of ICBA in the LBP is found in the sample when a co-solvent in which the polymer is selectively soluble (BB) is used; while a morphology with ICBA phase separation is formed when a co-solvent in which ICBA is selectively soluble (CP) is used. The volume fraction and mean size of the ICBA aggregates increases, while the size polydispersity of the ICBA aggregates decreases, with an increase in the amount of 2-chlorophenol as a co-solvent in the solution prior to film deposition. Moreover, these results therefore require that the interactions between PCPDTBT and ICBA, rather than the interactions between either of these components and the solvent, dominate the morphology development during deposition.

© 2014 WILEY-VCH Verlag GmbH & Co. KGaA, Weinheim

Furthermore, this work shows a significant improvement of LBP:fullerene device performance without a change in polymer ordering, which presents a unique system that indicates the crucial role of the presence of fullerene aggregates on device performance, even in the absence of increased polymer ordering. Further quantitative analysis also shows that the interfacial area between ICBA aggregates and its surrounding matrix correlates directly to the improvement of device performance.

More importantly, the judicious choice of solvent provides a level of morphological control in LBP:ICBA mixtures that has not been previously available. This novel process, therefore, precisely guides the morphology development in LBP:ICBA active layers and offers a promising process to increase power conversion efficiency.

5. Experimental Section

ICBA was purchased from Sigma Aldrich, and PCPDTBT (M_W = 34 K, PDI = 2.2) was purchased from 1-Materials. To fabricate the PCPDTBT/ICBA films, PCPDTBT (7 mg/ml) and ICBA (14 mg/ml) were dissolved in either *o*-dichlorobenzene (ODCB) or ODCB with varying amounts of a second solvent. Two co-solvents, bromobenzene (BB) and 2-chlorophenol (CP), were used in this work. PCPDTBT is selectively soluble in bromobenzene, while ICBA is selectively soluble in CP. The solubility of ICBA and PCPDTBT in ODCB are similar. The solubility of PCPDTBT in BB, ODCB, and CP was determined in our previous work[34] while the solubility of ICBA in BB, ODCB and CP is measured by the same UV–Vis procedure as previously described, with the results presented in the Supporting Information. The active layer was fabricated by spin casting a thin film from the PCPDTBT/ICBA solution at 1000 rpm for 60 s. Prior to spin-coating, the silicon wafers are cleaned by immersion in a 3:1 (v/v) mixture of concentrated sulfuric acid and hydrogen peroxide, heated to ≈70 °C for 15 min, and rinsed with copious amounts of high purity water and dried under a stream of nitrogen.

Small Angle Neutron Scattering: The small angle neutron scattering experiments (SANS) were completed on the General Purpose SANS instrument at the High Flux Isotope Reactor at Oak Ridge National Laboratory. The raw data were corrected for scattering from the empty cell, detector dark current, and detector sensitivity. The corrected data were then normalized to an absolute scale using a Porasil-A standard. A stack of 12 or more spin-coated layers was used for each SANS experiment. The scattering length density (SLD) of PCPDTBT is 1.1×10^{-6} Å^{-2},[35] while the SLD of ICBA is 4.17×10^{-6} Å^{-2}, which was determined by the measurement of the neutron reflectivity of an ICBA thin film and verified by calculating the SLD based on the mass density of ICBA and its atomic composition. The density of PCPDTBT and ICBA are 1.10 g/cm^3 and 1.44 g/cm^3, respectively.[35,36]

Neutron Reflectometry: All reflectivity measurements on the thin films were completed on the Liquids Reflectometer at the Spallation Neutron Source at Oak Ridge National Laboratory. The measured reflectivity curves of the samples are fitted with the calculated reflectivity of the model scattering length density profiles using Layers[37] and Motofit Software[38] to determine the structure of the thin films. In the fitting procedure, the scattering length density, thickness, and roughness of each layer are freely varied. A model is assumed to accurately reflect the structure of the sample when the model reflectivity profile converges with the experimental profile, where the quality of fit is gauged using χ^2 statistics, and the mass balance of the model system is within 5% of the mass balance of the sample. The SLD profile is then analyzed to obtain the concentration depth profile of each component in the system. For instance, the ICBA concentration depth profile is determined using

$$\phi(z)_{\mathrm{ICBA}} = \frac{\rho(z) - \rho_{\mathrm{PCPDTBT}}}{\rho_{\mathrm{ICBA}} - \rho_{\mathrm{PCPDTBT}}} \quad (1)$$

where $\Phi(z)_{\mathrm{ICBA}}$ is the volume fraction of ICBA at depth z, $\rho(z)$ is the experimental scattering length density at depth z, and ρ_{PCPDTBT} and ρ_{ICBA} are the SLD of PCPDTBT and ICBA, respectively. UV–Vis spectra were recorded with a Thermo Scientific Evolution 600 UV–Vis spectrophotometer with wavelength from 500 nm to 900 nm. The sample consists of a thin film of a PCPDTBT:ICBA blend that was spun-cast onto a glass substrate, where the reported spectrum of all the samples were obtained after subtracting the spectrum of the glass substrate. The same UV–Vis procedure as previously described is used to determine the solubility of the fullerene in the different solvents.[34]

Photovoltaic Device Fabrication and Characterization: Indium tin oxide (ITO) glass substrates were first washed with detergent and then cleaned in an ultrasonic bath using DI water, acetone and isopropyl alcohol (IPA), which was followed by the UV Ozone treatment for 20 min. Device was fabricated with a standard architecture ITO/PEDOT:PSS/BHJ/Ca/Al. The PEDOT:PSS film was then fabricated by spin coating PEDOT:PSS (Baytron P 4083) on the UV-treated ITO glass at 4000 rpm for 40 s and subsequently annealed in air at 140 °C for 20 min. The active layer was spin cast at the same condition as above. Finally, to create the OPV device, 40 nm of Ca and 60 nm of Al were thermally deposited on the film through a shadow mask. The current–voltage (*I–V*) measurements of the polymer photovoltaic cells were conducted using a Thermal Oriel 96000 300-W solar simulator under the lumination of AM1.5G, 100 mW/cm^2.

Acknowledgements

The authors wish to acknowledge the Sustainable Energy Education Research Center and the Joint Institute for Neutron Sciences at the University of Tennessee, as well as the National Science Foundation (DMR-1005987) for support of this project. MDD also acknowledges the support of the Department of Energy, Office of Basic Energy Sciences, Division of Materials Sciences and Engineering. The support of the Scientific User Facilities Division, Office of Basic Energy Sciences, U.S. Department of Energy, who sponsors the Oak Ridge National Laboratory High Flux Isotope Reactor and Spallation Neutron Source is gratefully acknowledged.

Received: May 1, 2014
Revised: August 14, 2014
Published online: September 16, 2014

[1] G. Yu, J. Gao, J. C. Hummelen, F. Wudl, A. J. Heeger, *Science* **1995**, *270*, 1789.
[2] J. Peet, J. Y. Kim, N. E. Coates, W. L. Ma, D. Moses, A. J. Heeger, G. C. Bazan, *Nat. Mater.* **2007**, *6*, 497.
[3] G. Li, V. Shrotriya, Y. Yao, J. S. Huang, Y. Yang, *J. Mater. Chem.* **2007**, *17*, 3126.
[4] G. Li, V. Shrotriya, J. S. Huang, Y. Yao, T. Moriarty, K. Emery, Y. Yang, *Nat. Mater.* **2005**, *4*, 864.
[5] S. Günes, H. Neugebauer, N. S. Sariciftci, *Chem. Rev.* **2007**, *107*, 1324.
[6] G. Zhao, Y. He, Y. Li, *Adv. Mater.* **2010**, *22*, 4355.
[7] Y. He, H. Y. Chen, Y. Hou,Y. Li , *J. Am. Chem. Soc.* **2010**, *132*, 1377.
[8] N. C. Miller, S. Sweetnam, E. R. Hoke, G. Roman, C. E. Miller, J. A. Bartelt, X. X. Xie, M. F. Toney, M. D. McGehee, *Nano Lett.* **2012**, *12*, 1566.
[9] H. Azimi, D. Fournier, M. Wirix, E. Dobrocka, T. Ameri, F. Machui, S. Rodman, G. Dennler, M. C. Scharber, K. Hingerl, J. Loos, C. J. Brabec, M. Morana, *Org. Electron.* **2012**, *13*, 1315.
[10] E. T. Hoke, K. Vandewal, J. A. Bartelt, W. R. Mateker, J. D. Douglas, R. Noriega, K. R. Graham, J. M. J. Frechet, A. Salleo, M. D. McGehee, *Adv. Energy Mater.* **2013**, *3*, 220.
[11] G. Q. Ren, C. W. Schlenker, E. Ahmed, S. Subramaniyan, S. Olthof, A. Kahn, D. S. Ginger, S.A. Jenekhe, *Adv. Funct. Mater.* **2013**, *23*, 1238.

© 2014 WILEY-VCH Verlag GmbH & Co. KGaA, Weinheim

[12] M. A. Faist, S. Shoaee, S. Tuladhar, G. F. A. Dibb, S. Foster, W. Gong, T. Kirchartz, S. D. C. Bradley, J. R. Durrant, J. Nelson, *Adv. Energy Mater.* **2013**, *3*, 744.
[13] S. Yamamoto, A. Orimo, H. Ohkita, H. Benten, S. Ito, *Adv. Energy Mater.* **2012**, *2*, 229.
[14] Y. Gu, C. Wang, T. P. Russell, *Adv. Energy Mater.* **2012**, *2*, 683.
[15] T. Wang, A. J. Pearson, A. D. F. Dunbar, P. A. Staniec, D. C. Watters, H. Yi, A. J. Ryan, R. A. J. Jones, A. Iraqi, D. G. Lidzey, *Adv. Funct. Mater.* **2012**, *22*, 1399.
[16] Z. M. Beiley, E. T. Hoke, R. Noriega, J. Dacuna, G. F. Burkhard, J. A. Bartelt, A. Salleo, M. F. Toney, M. D. McGehee, *Adv. Energy Mater.* **2011**, *1*, 954.
[17] S. J. Lou, J. M. Szarko, T. Xu, L. P. Yu, T. J. Marks, L. X. Chen, *J. Am. Chem. Soc.* **2011**, *133*, 20661.
[18] Y. Y. Liang, Z. Xu, J. B. Xia, S. Tsai, Y. Wu, G. Li, C. Ray, L. P. Lu, *Adv. Mater.* **2010**, *22*, E135.
[19] K. R. Graham, P. M. Wieruszewski, R. Stalder, M. J. Hartel, J. G. Mei, F. So, J. R. Reynolds, *Adv. Funct. Mater.* **2012**, *22*, 4801.
[20] H. P. Chen, J. H. Chen, W. Yin, X. Yu, M. Shao, K. Xiao, K. L. Hong, D. L. Pickel, W. M. Kochemba, S. M. Kilbey II, M. Dadmun, *J. Mater. Chem. A* **2013**, *1*, 5309.
[21] W. Yin, M. Dadmun, *ACS Nano* **2011**, *5*, 4756.
[22] J. W. Kiel, A. P. R. Eberle, M. E. Mackay, *Phys. Rev. Lett.* **2010**, *105*, 168701.
[23] J. Peet, N. S. Cho, S. K. Lee, G. C. Bazan, *Macromolecules* **2008**, *41*, 8655.
[24] Y. Yao, J. H. Hou, Z. Xu, G. Li, Y. Yang, *Adv. Funct. Mater.* **2008**, *18*, 1783.
[25] H. Y. Chen, H. Yang, G. Yang, S. Sista, R. Zadoyan, G. Li, Y. Yang, *J. Phys. Chem. C* **2009**, *113*, 7946.
[26] A. J. Parnell, A. D. F. Dunbar, A. J. Pearson, P. A. Staniec, A. J. C. Dennison, H. Hamamatsu, M. W. A. Skoda, D. G. Lidzey, R. A. L. Jones, *Adv. Mater.* **2010**, *22*, 2444.
[27] H. P. Chen, R. Hegde, J. Browning, M. D. Dadmun, *Phys. Chem. Chem. Phys.* **2012**, *14*, 5635.
[28] G. V. Schulz, *Z. Phys. Chem.* **1939**, *B43*, 25.
[29] H. P. Chen, S. Hu, H. D. Zang, B. Hu, M. Dadmun, *Adv. Funct. Mater.* **2013**, *23*, 1701.
[30] N. D. Treat, C. G. Shuttle, M. F. Toney, C. J. Hawker, M. L. Chabinyc, *J. Mater. Chem.* **2011**, *21*, 15224.
[31] H. Y. Lu, B. Akgun, T. P. Russell, *Adv. Energy Mater.* **2011**, *1*, 870.
[32] F. Liu, Y. Gu, C. Wang, W. Zhao, D. Chen, A. L. Briseno, T. P. Russell, *Adv. Mater.* **2012**, *24*, 3947.
[33] N. Shin, L. J. Richter, A. A. Herzing, R. J. Kline, D. M. Delongchamp, *Adv. Energy Mater.* **2013**, *3*, 983.
[34] H. P. Chen, Y. C. Hsiao, B. Hu, M. Dadmun, *Adv. Funct. Mater.* **2014**, *24*, 5129.
[35] H. P. Chen, J. Peet, S. Hu, J. Azoulay, G. Baza, M. D. Dadmun, *Adv. Funct. Mater.* **2014**, *24*, 140.
[36] H. P. Chen, J. Peet, Y. C. Hsiao, B. Hu, M. Dadmun, *Chem. Mater.* **2014**, *26*, 3993.
[37] Layers is an Excel spreadsheet for modeling NR data developed by John Ankner at Oak Ridge National Laboratory.
[38] A. Nelson, *J. Appl. Cryst.* **2006**, *39*, 273.

© 2014 WILEY-VCH Verlag GmbH & Co. KGaA, Weinheim